

Convective effects on a propagating reaction front

K. A. Cliffe

AEA Technology, Harwell, Didcot, Oxon. OX11 0RA, United Kingdom

S. J. Tavener

Department of Mathematics, Penn State, University Park, Pennsylvania 16802

H. Wilke

Institute of Crystal Growth, Berlin, Germany

(Received 9 July 1997; accepted 3 November 1997)

Unstable concentration gradients inherent in traveling chemical waves can give rise to buoyancy-driven convection, altering the speed of the wave. When an excitable Belousov–Zhabotinsky reaction system is confined within a sufficiently narrow, vertical two-dimensional channel, convection arises at a symmetry-breaking bifurcation point. The observed linear rate of change of wave speed with the bifurcation parameter is a necessary consequence of the Z_2 symmetry present. © 1998 American Institute of Physics. [S1070-6631(98)00303-1]

I. INTRODUCTION

The experiments of Bazsa and Epstein,¹ Pojman and Epstein,² Masere *et al.*³ and the subsequent computations of Wu *et al.*⁴ and Zhang *et al.*,⁵ demonstrate the intriguing nature of chemical waves traveling vertically in tubes and channels containing excitable Belousov–Zhabotinsky reaction mixtures. Below a critical tube diameter, both ascending and descending waves travel at the same speed, which is independent of tube diameter. Above this critical diameter, for certain initial reactant concentrations, the wave speed of the ascending wave increases linearly with tube diameter, while the speed of the descending wave remains unchanged. For different reactant concentrations, the speeds of both ascending and descending waves vary linearly with tube diameter. The rate of change of wave speed with tube diameter may be different for ascending and descending waves, but this could not be confirmed within experimental error.² Non-planar, distorted wave fronts are found to be associated with the different wave speeds. When experiments are performed in silica gel or when glass beads are introduced into the tubes, the speed of both ascending and descending waves are equal and constant with respect to changes in tube diameter. It seems clear that the changes in wave speed and the distortion of the wave front are the result of convection driven by the density gradients associated with the traveling chemical wave.

In this study we observe that the onset of convection in vertical channels occurs as a bifurcation from the nonconfecting solution. This perspective allows numerical bifurcation techniques to be used to map loci of critical conditions in the multidimensional parameter space. The linear dependence of wave speed on channel width is shown to be a necessary consequence of the midchannel symmetry. We examine four distinct instability mechanisms that arise and show why convection need not necessarily increase the speed of the wave, but can slow the wave in some circumstances. We justify the differences between the rates of change of

wave speed with channel width for ascending and descending waves. Finally, we consider the influence of the small parameter ϵ on the speed of the reaction-diffusion wave and on the critical Grashof numbers at which convection arises. A preliminary investigation of the interaction between ϵ , convection, and wave speed is reported.

II. THE TWO-DIMENSIONAL (2-D) MODEL

Simplifying the experimental problem in the same manner as Wu *et al.*⁴ and Zhang *et al.*,⁵ we consider the Belousov–Zhabotinsky reaction to occur in a vertical *two-dimensional* slot. We define our coordinate system so that the origin is centrally located along the bottom of the slot, with the x axis pointing vertically upward and the y axis pointing across the channel. The two-species Oregonator model is used to approximate the BZ reaction kinetics. If t_0 is the time scale inherent in the Oregonator model, we define length scale x_0 so as to make the nondimensional diffusion coefficient D_1 [defined in Eq. (8) below as $D_1 = d_1 t_0 / x_0^2$] to be equal to 1. We nondimensionalize the coupled Navier–Stokes and reaction equations with respect to length scale x_0 and diffusive time scale x_0^2 / ν , where ν is the kinematic viscosity. Taking the usual value of $x_0 = 0.018$ cm (Jahnke, Skaggs, and Winfree⁶) and using a nominal value of 0.01 cm²/s for the kinematic viscosity of water, our time scale is 0.0324 s and our velocity scale is therefore $u_0 = \nu / x_0 = 0.56$ cm/s or 333 mm/min. To allow for slots of different widths, we rescale the y direction by a variable width σ and correspondingly rescale the y component of velocity so as to retain the simple form of the continuity equation (3). Böckmann *et al.*⁷ conclude that the temperature gradients associated with the wave can be neglected for typical ferroin-catalyzed BZ systems. They have shown that a maximum temperature difference of only 50 mK exists for these systems and that chemically induced density changes are dominant. Further, since the thermal diffusivity is large

when compared to the diffusivities of the chemical species, an isothermal approximation seems appropriate.

Using the nondimensionalization described above, the coupled Navier–Stokes equations and the Oregonator model become

$$D_\nu \left(\frac{\partial u}{\partial t} + u \frac{\partial u}{\partial x} + v \frac{\partial u}{\partial y} \right) = D_\nu \left(-\frac{\partial p}{\partial x} + \frac{\partial^2 u}{\partial x^2} + \frac{1}{\sigma^2} \frac{\partial^2 u}{\partial y^2} \right) - D_\nu (\text{Gr}_1 c_1 + \text{Gr}_2 c_2), \quad (1)$$

$$\sigma D_\nu \left(\frac{\partial v}{\partial t} + u \frac{\partial v}{\partial x} + v \frac{\partial v}{\partial y} \right) = D_\nu \left(-\frac{1}{\sigma} \frac{\partial p}{\partial y} + \sigma \frac{\partial^2 v}{\partial x^2} + \frac{1}{\sigma} \frac{\partial^2 v}{\partial y^2} \right), \quad (2)$$

$$\frac{\partial u}{\partial x} + \frac{\partial v}{\partial y} = 0, \quad (3)$$

$$\epsilon D_\nu \left(\frac{\partial c_1}{\partial t} + u \frac{\partial c_1}{\partial x} + v \frac{\partial c_1}{\partial y} \right) = \epsilon D_1 \left(\frac{\partial^2 c_1}{\partial x^2} + \frac{1}{\sigma^2} \frac{\partial^2 c_1}{\partial y^2} \right) + c_1 - c_1^2 - f c_2 \left(\frac{c_1 - q}{c_1 + q} \right), \quad (4)$$

$$D_\nu \left(\frac{\partial c_2}{\partial t} + u \frac{\partial c_2}{\partial x} + v \frac{\partial c_2}{\partial y} \right) = D_2 \left(\frac{\partial^2 c_2}{\partial x^2} + \frac{1}{\sigma^2} \frac{\partial^2 c_2}{\partial y^2} \right) + c_1 - c_2, \quad (5)$$

where u, v are the nondimensional velocities in the x and y directions, respectively, p is the nondimensional (reduced) pressure, $c_i, i=1,2$ is the scaled concentration of chemical species i as defined in the Oregonator model and \mathbf{g} is the gravity vector. The nondimensional groups are

$$D_\nu = \frac{\nu t_0}{x_0^2}, \quad (6)$$

$$\text{Gr}_i = \frac{g x_0^3}{\nu^2} \left(\frac{\rho_i - \rho_0}{\rho_0} \right), \quad i=1,2, \quad (7)$$

$$D_i = \frac{d_i t_0}{x_0^2}, \quad i=1,2, \quad (8)$$

where $g = \|\mathbf{g}\|_2$, density $\rho = \rho_0 + \rho_1 c_1 + \rho_2 c_2$, where ρ_i is the density of chemical species i , and d_i is the (dimensional) diffusivity of chemical species i . The small parameter ϵ is dependent upon reaction constants and upon the initial concentrations of bromate ion, malonic acid and H^+ . It reflects the two different time scales inherent in the chemical kinetics. The stoichiometric factor f represents the number of bromide ions liberated for every two metal oxide ions reduced and q is a ratio of reaction constants.

This coupled system of five partial differential equations, previously described in Wilke,⁸ extends the system of Wu *et al.*,⁴ who consider one chemical species only and therefore, as we shall see, limit the types of instabilities that may arise.

III. THE SOLUTION METHOD

Rather than solve Eqs. (1)–(5) with appropriate boundary and initial conditions directly, we seek solutions in the

form of a traveling wave propagating in the positive x direction with constant speed ω , i.e., a solution of the form

$$u(x - \omega t, y), \quad v(x - \omega t, y), \quad p(x - \omega t, y), \\ c_1(x - \omega t, y), \quad c_2(x - \omega t, y), \quad (9)$$

or

$$u(\eta, y), \quad v(\eta, y), \quad p(\eta, y), \quad c_1(\eta, y), \\ c_2(\eta, y), \quad \text{where } \eta = x - \omega t. \quad (10)$$

Equations (1)–(5) become

$$D_\nu \left(-\omega \frac{\partial u}{\partial \eta} + u \frac{\partial u}{\partial \eta} + v \frac{\partial u}{\partial y} \right) = D_\nu \left(-\frac{\partial p}{\partial \eta} + \frac{\partial^2 u}{\partial \eta^2} + \frac{1}{\sigma^2} \frac{\partial^2 u}{\partial y^2} \right) - D_\nu (\text{Gr}_1 c_1 + \text{Gr}_2 c_2), \quad (11)$$

$$\sigma D_\nu \left(-\omega \frac{\partial v}{\partial \eta} + u \frac{\partial v}{\partial \eta} + v \frac{\partial v}{\partial y} \right) = D_\nu \left(-\frac{1}{\sigma} \frac{\partial p}{\partial y} + \sigma \frac{\partial^2 v}{\partial \eta^2} + \frac{1}{\sigma} \frac{\partial^2 v}{\partial y^2} \right), \quad (12)$$

$$\frac{\partial u}{\partial \eta} + \frac{\partial v}{\partial y} = 0, \quad (13)$$

$$\epsilon D_\nu \left(-\omega \frac{\partial c_1}{\partial \eta} + u \frac{\partial c_1}{\partial \eta} + v \frac{\partial c_1}{\partial y} \right) = \epsilon D_1 \left(\frac{\partial^2 c_1}{\partial \eta^2} + \frac{1}{\sigma^2} \frac{\partial^2 c_1}{\partial y^2} \right) + c_1 - c_1^2 - f c_2 \left(\frac{c_1 - q}{c_1 + q} \right), \quad (14)$$

$$D_\nu \left(-\omega \frac{\partial c_2}{\partial \eta} + u \frac{\partial c_2}{\partial \eta} + v \frac{\partial c_2}{\partial y} \right) = D_2 \left(\frac{\partial^2 c_2}{\partial \eta^2} + \frac{1}{\sigma^2} \frac{\partial^2 c_2}{\partial y^2} \right) + c_1 - c_2. \quad (15)$$

We solve this system of equations in the domain

$$\Omega = \{(\eta, y) : 0 \leq \eta \leq 100, -0.5 \leq y \leq 0.5\}, \quad (16)$$

with boundary Γ . Non-slip boundary conditions are applied along the channel walls and at the bottom, which part of the boundary we denote Γ_D , i.e.,

$$u = v = 0 \quad \text{on } \eta = 0 \quad \text{and} \quad y = \pm 0.5, \quad (17)$$

where u, v are the velocities in the *laboratory* frame. We further require that the normal derivatives of the concentrations vanish at the boundary, i.e.,

$$\frac{\partial c_i}{\partial n} = 0, \quad i=1,2 \quad \text{on } \Gamma. \quad (18)$$

A convenient way in which to calculate the unknown (*constant*) velocity ω when using the finite-element package ENTWIFE⁹ is to solve Laplace's equation in Ω with natural boundary conditions on Γ , i.e.,

$$\nabla^2 \omega = \frac{\partial^2 \omega}{\partial \eta^2} + \frac{1}{\sigma^2} \frac{\partial^2 \omega}{\partial y^2} = 0, \quad \text{in } \Omega, \quad (19)$$

with

$$\frac{\partial \omega}{\partial n} = 0, \quad \text{on } \Gamma. \quad (20)$$

This can then be solved like any other elliptic partial differential equation, and further ensures that the wave speed ω is known on every element of the discretization.

Weak equations can be constructed in the usual manner, and we seek steady solutions,

$$[\mathbf{u}(\eta, y), p(\eta, y), c_1(\eta, y), c_2(\eta, y), \omega(\eta, y)],$$

such that $\mathbf{u} \in V_0, p \in L_0^2, c_1, c_2, \omega \in W$,

where

$$V_0 = \{\mathbf{v} \in \mathbf{H}^1(\Omega) : \mathbf{v} = \mathbf{0} \text{ on } \Gamma_D\}, \quad (21)$$

$$L_0^2 = \left\{ q \in L^2(\Omega) : \int_{\Omega} q \, dA = 0 \right\}, \quad (22)$$

$$W = \left\{ w \in H^1(\Omega) : \frac{\partial w}{\partial n} = 0 \text{ on } \Gamma \right\}, \quad (23)$$

and

$$\int_{\Omega} D_v \left(-\omega \frac{\partial u}{\partial \eta} + u \frac{\partial u}{\partial \eta} + v \frac{\partial u}{\partial y} + \text{Gr}_1 c_1 + \text{Gr}_2 c_2 \right) \chi_u \, dA$$

$$+ \int_{\Omega} D_v \left[\left(-p + \frac{\partial u}{\partial \eta} \right) \frac{\partial \chi_u}{\partial \eta} + \frac{1}{\sigma^2} \frac{\partial u}{\partial y} \frac{\partial \chi_u}{\partial y} \right] dA = 0, \quad (24)$$

$$\int_{\Omega} \sigma D_v \left(-\omega \frac{\partial v}{\partial \eta} + u \frac{\partial v}{\partial \eta} + v \frac{\partial v}{\partial y} \right) \chi_v \, dA$$

$$+ \int_{\Omega} D_v \left[\sigma \frac{\partial v}{\partial \eta} \frac{\partial \chi_v}{\partial \eta} + \frac{1}{\sigma} \left(-p + \frac{\partial v}{\partial y} \right) \frac{\partial \chi_v}{\partial y} \right] dA = 0, \quad (25)$$

$$\int_{\Omega} \left(\frac{\partial u}{\partial \eta} + \frac{\partial v}{\partial y} \right) \chi_p \, dA = 0, \quad (26)$$

$$\int_{\Omega} \left[\epsilon D_v \left(-\omega \frac{\partial c_1}{\partial \eta} + u \frac{\partial c_1}{\partial \eta} + v \frac{\partial c_1}{\partial y} \right) - c_1 + c_1^2 \right. \\ \left. + f c_2 \left(\frac{c_1 - q}{c_1 + q} \right) \right] \chi_{c_1} \, dA$$

$$+ \int_{\Omega} \epsilon D_1 \left(\frac{\partial c_1}{\partial \eta} \frac{\partial \chi_{c_1}}{\partial \eta} + \frac{1}{\sigma^2} \frac{\partial c_1}{\partial y} \frac{\partial \chi_{c_1}}{\partial y} \right) dA = 0, \quad (27)$$

$$\int_{\Omega} \left[D_v \left(-\omega \frac{\partial c_2}{\partial \eta} + u \frac{\partial c_2}{\partial \eta} + v \frac{\partial c_2}{\partial y} \right) - c_1 + c_2 \right] \chi_{c_2} \, dA$$

$$+ \int_{\Omega} D_2 \left(\frac{\partial c_2}{\partial \eta} \frac{\partial \chi_{c_2}}{\partial \eta} + \frac{1}{\sigma^2} \frac{\partial c_2}{\partial y} \frac{\partial \chi_{c_2}}{\partial y} \right) dA = 0, \quad (28)$$

$$- \int_{\Omega} \left(\frac{\partial \omega}{\partial \eta} \frac{\partial \chi_{\omega}}{\partial \eta} + \frac{1}{\sigma^2} \frac{\partial \omega}{\partial y} \frac{\partial \chi_{\omega}}{\partial y} \right) dA = 0, \quad (29)$$

for all test functions,

$$\begin{pmatrix} \chi_u \\ \chi_v \end{pmatrix} \in V_0, \quad \chi_p \in L_0^2, \quad \chi_{c_1}, \chi_{c_2}, \chi_{\omega} \in W.$$

The above weak equations were solved via the finite-element method using isoparametric quadrilateral elements with biquadratic interpolation of the velocity field, chemical concentrations and wave speed, and discontinuous linear interpolation of the pressure field. The phase of the wave was fixed by replacing one of the equations for the velocity ω with a Dirichlet condition for c_1 at an appropriate node. The resulting nonlinear system of equations may be written as

$$\mathbf{f}(\mathbf{x}, \lambda) = \mathbf{0}, \quad \mathbf{f}: \mathbb{R}^N \times \mathbb{R}^p \rightarrow \mathbb{R}^N, \quad (30)$$

which was solved using Newton's method. In the absence of convection, u , v , p , c_1 , and c_2 are all independent of the cross channel direction y . An initial guess for the nonconvecting solution was obtained from a one-dimensional finite-difference computation. This gave both a sufficiently accurate initial guess to enable the Newton iteration to converge, and allowed a finite-element mesh to be designed that accurately approximated the steep concentration gradients present.

A. Discretization of the pressure field

When $u = v = 0$, a balance exists between the species concentrations and the pressure gradient. Since this "hydrostatic" pressure field is nontrivial and expensive to compute, we choose to absorb it into the reduced pressure and compute only the *difference* in the pressure field between nonconvecting and convecting solutions. From Eqs. (11) and (12), we see that when $u(\eta, y) = v(\eta, y) = 0$,

$$\frac{\partial p}{\partial \eta} = -(\text{Gr}_1 c_1 + \text{Gr}_2 c_2) \quad \text{and} \quad \frac{\partial p}{\partial y} = 0.$$

Let

$$b_1(\eta) = c_1(\eta, y), \quad \text{when } u = v = 0,$$

$$b_2(\eta) = c_2(\eta, y), \quad \text{when } u = v = 0,$$

noting that b_1 and b_2 are independent of y . Now define

$$\hat{p}(\eta, y) = p(\eta, y) + \int (\text{Gr}_1 b_1 + \text{Gr}_2 b_2) d\eta, \quad (31)$$

so that

$$\frac{\partial \hat{p}}{\partial \eta} = \frac{\partial p}{\partial \eta} + (\text{Gr}_1 b_1 + \text{Gr}_2 b_2),$$

$$\frac{\partial \hat{p}}{\partial y} = \frac{\partial p}{\partial y}.$$

Equations (11) and (12) become

$$D_v \left(-\omega \frac{\partial u}{\partial \eta} + u \frac{\partial u}{\partial \eta} + v \frac{\partial u}{\partial y} \right)$$

$$= D_v \left(-\frac{\partial \hat{p}}{\partial \eta} + \frac{\partial^2 u}{\partial \eta^2} + \frac{1}{\sigma^2} \frac{\partial^2 u}{\partial y^2} \right)$$

$$- D_v [\text{Gr}_1 (c_1 - b_1) + \text{Gr}_2 (c_2 - b_2)], \quad (32)$$

$$\begin{aligned} \sigma D_\nu \left(-\omega \frac{\partial v}{\partial \eta} + u \frac{\partial v}{\partial \eta} + v \frac{\partial v}{\partial y} \right) \\ = D_\nu \left(-\frac{1}{\sigma} \frac{\partial \hat{p}}{\partial y} + \sigma \frac{\partial^2 v}{\partial \eta^2} + \frac{1}{\sigma} \frac{\partial^2 v}{\partial y^2} \right). \end{aligned} \quad (33)$$

We compute and store $b_1(\eta)$ and $b_2(\eta)$. The pressure field $\hat{p}(\eta, y) \equiv 0$ for *all* nonconvecting solutions, independently of Gr_1 and Gr_2 .

B. The role of the midchannel symmetry

The finite-dimensional equations (30) are equivariant with respect to an $(N \times N)$ orthogonal matrix S , such that $S^2 = I$, but $S \neq I$, i.e.

$$S\mathbf{f}(\mathbf{x}, \lambda) = \mathbf{f}(S\mathbf{x}, \lambda). \quad (34)$$

The orthogonal matrix S induces a unique decomposition of \mathbb{R}^N into symmetric and antisymmetric subspaces,

$$\mathbb{R}^N = \mathbb{R}_s^N \oplus \mathbb{R}_a^N,$$

where

$$\mathbb{R}_s^N = \{\mathbf{x} \in \mathbb{R}^N : S\mathbf{x} = \mathbf{x}\},$$

$$\mathbb{R}_a^N = \{\mathbf{x} \in \mathbb{R}^N : S\mathbf{x} = -\mathbf{x}\}.$$

Symmetric solutions are those for which

$$u(\eta, y) = u(\eta, -y), \quad v(\eta, y) = -v(\eta, -y),$$

$$p(\eta, y) = p(\eta, -y),$$

$$c_1(\eta, y) = c_1(\eta, -y), \quad c_2(\eta, y) = c_2(\eta, -y),$$

$$\omega(\eta, y) = \omega(\eta, -y).$$

Antisymmetric solutions are therefore those for which

$$u(\eta, y) = -u(\eta, -y), \quad v(\eta, y) = v(\eta, -y),$$

$$p(\eta, y) = -p(\eta, -y),$$

$$c_1(\eta, y) = -c_1(\eta, -y), \quad c_2(\eta, y) = -c_2(\eta, -y),$$

$$\omega(\eta, y) = -\omega(\eta, -y).$$

Nonconvecting flows, which are symmetric, were computed on

$$\Omega^- = \{(\eta, y) : 0 \leq \eta \leq 100, -0.5 \leq y \leq 0\}, \quad (35)$$

with the appropriate symmetry boundary conditions along $y=0$.

At a simple symmetry-breaking bifurcation point $(\mathbf{x}^0, \lambda^0)$,

$$\mathbf{x}^0 \in \mathbb{R}_s^N,$$

$$\text{Null}(\mathbf{f}_x^0) = \text{span}\{\phi\}, \quad \phi \in \mathbb{R}_a^N, \quad \phi \neq \mathbf{0},$$

$$\text{Range}(\mathbf{f}_x^0) = \{\mathbf{y} \in \mathbb{R}^N : \psi^T \mathbf{y} = 0\}, \quad \psi \in \mathbb{R}^N, \quad \psi \neq \mathbf{0},$$

where

$$\mathbf{f}_x^0 = \frac{\partial \mathbf{f}}{\partial \mathbf{x}}(\mathbf{x}^0, \lambda^0).$$

The onset of convection at a symmetry-breaking bifurcation point was computed as a regular solution of the extended system described by Werner and Spence,¹⁰ namely

$$\mathbf{F}(\mathbf{y}) = \begin{pmatrix} \mathbf{f} \\ \mathbf{f}_x \phi \\ \mathbf{I}^T \phi - 1 \end{pmatrix} = \mathbf{0}, \quad (36)$$

where

$$\mathbf{y}^T = (\mathbf{x}^T, \phi^T, \lambda), \quad \mathbf{y} \in (\mathbb{R}_s^N \times \mathbb{R}_a^N \times \mathbb{R}^1),$$

$$\mathbf{F} : \mathbb{R}_s^N \times \mathbb{R}_a^N \times \mathbb{R}^1 \rightarrow \mathbb{R}_s^N \times \mathbb{R}_a^N \times \mathbb{R}^1,$$

and $\mathbf{I} \in \mathbb{R}^N$ with $\mathbf{I} \neq \mathbf{0}$. All computations were performed using the finite-element package ENTWIFE.⁹

The Jacobian of the system of equations (30) must be calculated in order to find solutions using Newton's method. Given the complicated nature of the weak forms (24)–(29), this is obviously a nontrivial exercise. To follow a branch of solutions using arclength continuation, the derivatives of the discretized system (30) with respect to the parameters are required. Second-order derivatives with respect to both the variables and the parameters are necessary in order to construct and solve Eq. (36) via Newton's method, and then to perform continuation with respect to the desired parameter. The computer algebra system REDUCE¹¹ was used to produce the necessary subroutines to compute the required derivatives. This approach (or an equivalent one) was deemed to be absolutely essential in order to calculate these derivatives accurately.

IV. THE ONSET OF CONVECTION

The parameter values chosen for our initial investigation were

$$D_1 = 1, \quad D_2 = 0.6, \quad D_\nu = 600, \quad \epsilon = 0.1, \quad f = 3, \\ q = 0.0002, \quad \text{and} \quad \sigma = 2.$$

A value of $\epsilon = 0.1$, rather than the more usual values of 0.01 or 0.05, was chosen for the initial part of our study in order to ease some of the computational difficulties associated with the range of length scales present in the problem. As ϵ decreases, both the concentration gradients associated with the front and tail of the activator (species 1) wave increase, and the length of the tail of the inhibitor (species 2) wave increases. A larger value of ϵ was also found to make the competing effects of convection (to be discussed below) more obvious. Using the ‘‘Oregonator’’ length scale of $x_0 = 0.018$ cm, a width $\sigma = 2$ corresponds to a physical channel width of only 0.36 mm. Such a narrow channel was chosen at first so that the primary convective instability would be to a flow with a single roll across the channel. Instabilities with two rolls across the channel, which do *not* break the mid-channel symmetry described above, can occur as the primary instability for wider channels. For the region of parameter space examined here, these (symmetric) instabilities occur at larger Grashof numbers than the symmetry-breaking instability.

The concentrations of the activator and inhibitor species (c_1 and c_2 , respectively), in the nonconvecting solution, are

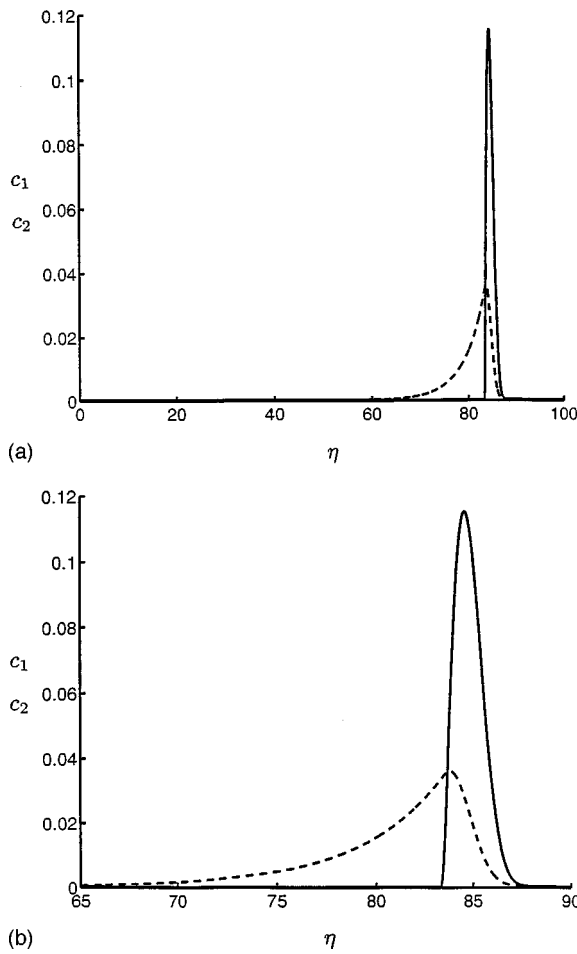


FIG. 1. (a) Species concentration profiles for the nonconvecting wave that travels with speed 2.32 mm/min, assuming $x_0=0.018$ cm and $\nu=0.01$ cm²/s. Here $\epsilon=0.1$, $D_1=1$, $D_2=0.6$, $D_\nu=600$, $f=3$, and $q=0.0002$. (b) Detail of species concentrations for the nonconvecting wave that travels with speed 2.32 mm/min, assuming $x_0=0.018$ cm and $\nu=0.01$ cm²/s. Here $\epsilon=0.1$, $D_1=1$, $D_2=0.6$, $D_\nu=600$, $f=3$, and $q=0.0002$.

shown in Figs. 1(a) and 1(b) as a function of η . For the values of the parameters we have chosen, the stable equilibrium concentrations are $c_1=c_2=3.9988 \times 10^{-4}$. The wave speed of the nonconvecting solution is 6.972×10^{-3} in our nondimensional units, corresponding to 2.32 mm/min (using a nominal value of 0.01 cm²/s for the kinematic viscosity).

The critical Grashof numbers at four distinct symmetry-breaking bifurcation points are listed in Table I. They were computed on Ω^- [defined by (35)], using 650 elements in the η direction and 24 elements between $y=-0.5$ and

TABLE I. Critical Grashof numbers for $D_1=1$, $D_2=0.6$, $D_\nu=600$, $\epsilon=0.1$, $f=3$, $q=0.0002$, and $\sigma=2$.

Gr_1	Gr_2
-1.99	0.0
0.998	0.0
0.0	-6.79
0.0	9.46

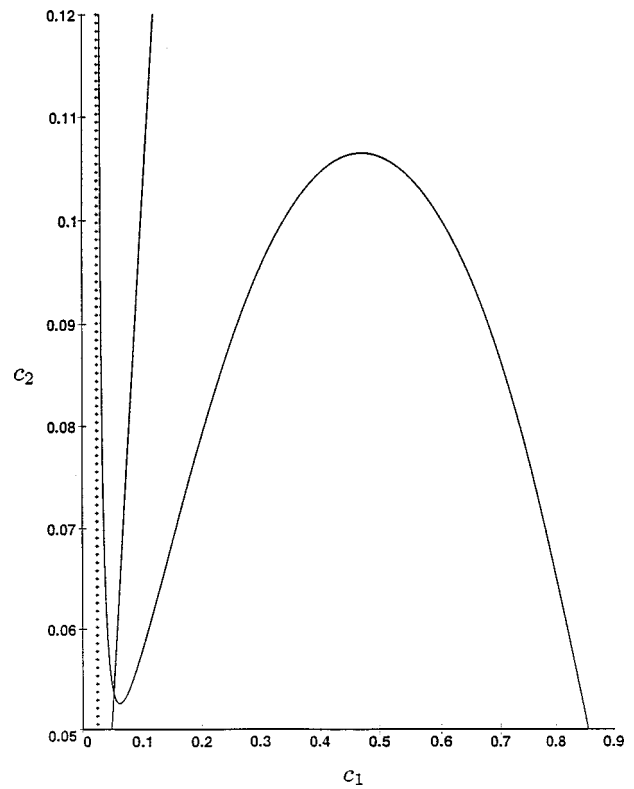


FIG. 2. Plot of the null clines of the two-component Oregonator model for $q=0.025$, $f=2.6$ for which the system is excitable.

$y=0$, and were unchanged to three significant figures from the values computed on a mesh with one-quarter of the number of elements.

The four different instability mechanisms at the bifurcation points in Table I are described below. Recall that since $f=3 > 1 + \sqrt{2}$, the Oregonator model is in an “excitable” state with the nullclines of the coupled ordinary differential equations qualitatively similar to those shown in Fig. 2.

When $Gr_1 = -1.99$ and $Gr_2 = 0$, species 1 is lighter than the bulk medium and species 2 is neutrally buoyant. The leading edge of the activator wave is gravitationally unstable and convection occurs ahead of the peak of c_1 , as illustrated by the equally spaced contours of the streamfunction corresponding to the null eigenvector, shown in Fig. 3(a). Only the part of the computational domain between $\eta=70$ and $\eta=95$ is shown. The vertical lines in this figure locate the maximum of c_1 and the values of η for which c_1 falls below 5% of its maximum excursion from the equilibrium value. Physically, when a parcel of heavy fluid ahead of the wave (which is at equilibrium) falls under the influence of gravity into the leading edge of the activator wave, its concentration of species 1 is increased by diffusion such that c_1 increases to the right of the minimum of the cubic-like isocline in Fig. 2. This triggers the fast (initiator) reaction that rapidly produces more of species 1, increasing c_1 and decreasing the density of the parcel of fluid. The parcel of fluid therefore tends to rise.

When $Gr_1=0.998$ and $Gr_2=0$, species 1 is heavier than the bulk medium and species 2 is neutrally buoyant. The trailing edge of the activator wave is gravitationally unstable

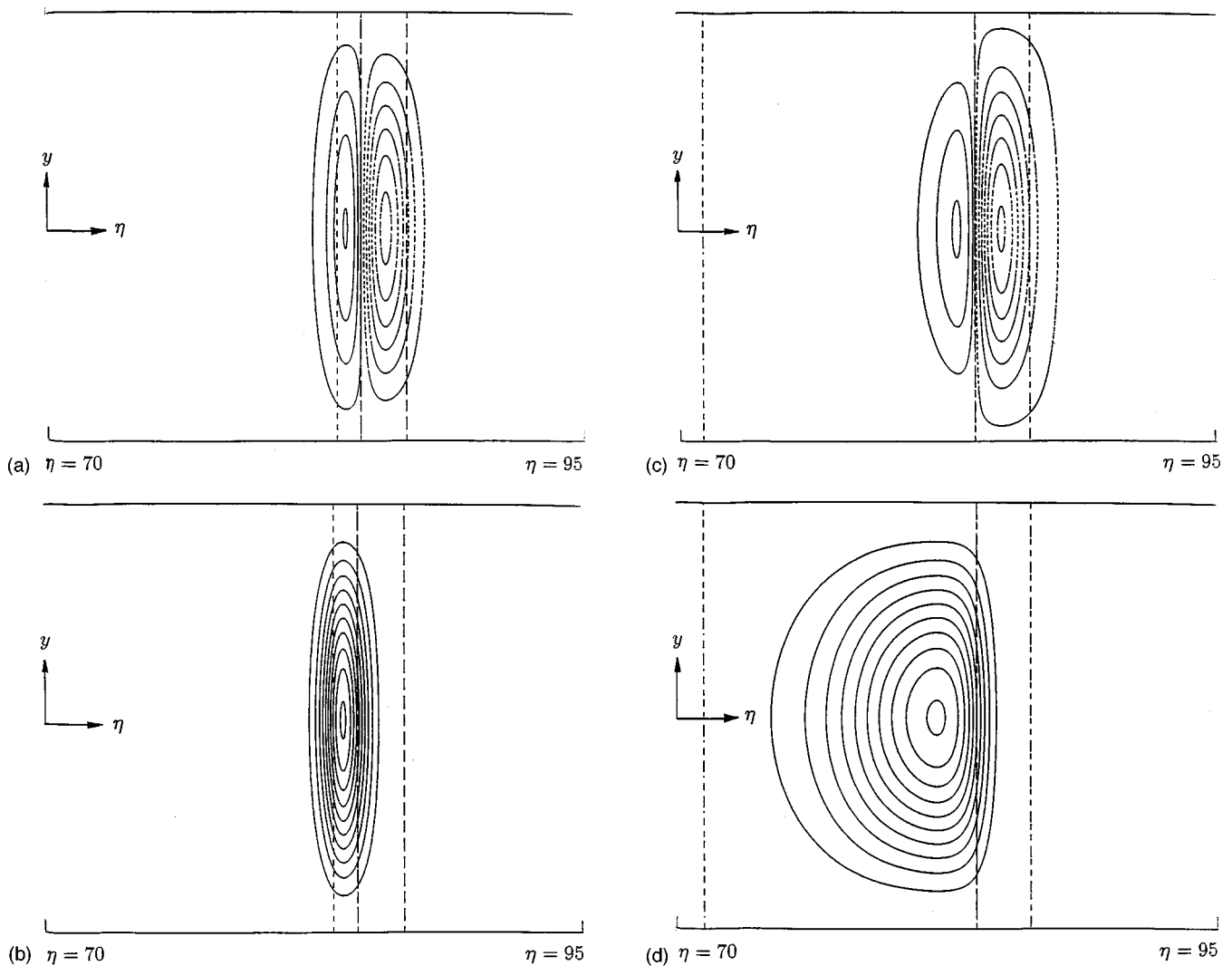


FIG. 3. (a) Streamfunction corresponding to the null eigenvector at $Gr_1 = -1.99$, $Gr_2 = 0$ at which the leading edge of the activator wave becomes linearly unstable. Here $\eta \in [70, 95]$, $y \in [-0.5, 0.5]$, and $\epsilon = 0.1$, $D_1 = 1$, $D_2 = 0.6$, $D_v = 600$, $f = 3$, $q = 0.0002$, and $\sigma = 2$. The vertical lines show the location of the maximum of c_1 and the positions at which c_1 relaxes below 5% of its maximum excursion from equilibrium. The streamfunction contours are equally spaced. (b) Streamfunction corresponding to the null eigenvector at $Gr_1 = 0.99$, $Gr_2 = 0$ at which the trailing edge of the activator wave becomes linearly unstable. Here $\eta \in [70, 95]$, $y \in [-0.5, 0.5]$, and $\epsilon = 0.1$, $D_1 = 1$, $D_2 = 0.6$, $D_v = 600$, $f = 3$, $q = 0.0002$, and $\sigma = 2$. The vertical lines show the location of the maximum of c_1 and the positions at which c_1 relaxes below 5% of its maximum excursion from equilibrium. The streamfunction contours are equally spaced. (c) Streamfunction corresponding to the null eigenvector at $Gr_1 = 0$, $Gr_2 = -6.79$ at which the leading edge of the inhibitor wave becomes linearly unstable. Here $\eta \in [70, 95]$, $y \in [-0.5, 0.5]$ and $\epsilon = 0.1$, $D_1 = 1$, $D_2 = 0.6$, $D_v = 600$, $f = 3$, $q = 0.0002$, and $\sigma = 2$. The vertical lines show the location of the maximum of c_2 and the positions at which c_2 relaxes below 5% of its maximum excursion from equilibrium. The streamfunction contours are equally spaced. (d) Streamfunction corresponding to the null eigenvector at $Gr_1 = 0$, $Gr_2 = 9.46$ at which the trailing edge of the inhibitor wave becomes linearly unstable. Here $\eta \in [70, 95]$, $y \in [-0.5, 0.5]$ and $\epsilon = 0.1$, $D_1 = 1$, $D_2 = 0.6$, $D_v = 600$, $f = 3$, $q = 0.0002$, and $\sigma = 2$. The vertical lines show the location of the maximum of c_2 and the positions at which c_2 relaxes below 5% of its maximum excursion from equilibrium. The streamfunction contours are equally spaced.

and convection arises behind the peak of c_1 , as illustrated by the streamfunction corresponding to the null eigenvector, shown in Fig. 3(b). When a parcel of heavy fluid in the trailing edge of the activator wave falls under the influence of gravity into the region behind the wave, its concentration of species 1 is decreased by diffusion, it becomes lighter and therefore tends to rise.

When $Gr_1 = 0$ and $Gr_2 = -6.79$, species 2 is lighter than the bulk medium and species 1 is neutrally buoyant. The leading edge of the inhibitor wave is gravitationally unstable and convection occurs ahead of the peak of c_2 , as illustrated by the streamfunction corresponding to the null eigenvector, shown in Fig. 3(c). The vertical lines locate the maximum of

c_2 and the values of η for which c_2 falls below 5% of its maximum excursion from the equilibrium value. When a parcel of heavy fluid at equilibrium falls under the influence of gravity into the leading edge of the inhibitor wave, its concentrations of species 1 and 2 are increased by diffusion, such that it moves to the right of the minimum of the cubic-like isocline in Fig. 2. This triggers the fast (initiator) reaction that rapidly produces more of the neutrally buoyant species 1, and also, although more slowly (or effectively later, if ϵ is very small), produces more of the lighter species 2. The parcel of fluid therefore tends to rise.

When $Gr_1 = 0$ and $Gr_2 = 9.46$, species 2 is heavier than the bulk medium and species 1 is neutrally buoyant. The

trailing edge of the inhibitor wave is gravitationally unstable and convection arises behind the peak of c_2 , as illustrated by the streamfunction corresponding to the null eigenvector, shown in Fig. 3(d). When a parcel of heavy fluid in the trailing edge of the inhibitor wave falls under the influence of gravity into the region behind the wave, which is at equilibrium, its concentration of species 2 is decreased by diffusion, it becomes lighter and therefore tends to rise.

The magnitudes of the critical values of Gr_1 in Table I suggest that the trailing edge of the activator wave is steeper than the leading edge. The magnitudes of the critical values for Gr_2 suggest that the leading edge of the inhibitor wave is steeper than the trailing edge and that both are much shallower than the corresponding leading and trailing edges of the activator wave. The critical Grashof numbers will obviously change if ϵ is varied and the shape of the reaction-diffusion wave changes. The relationship between the critical Grashof number and ϵ is further complicated by the fact that ϵ also effects the rate at which species 1 and 2 are produced once the reaction has been triggered. Since diffusion is involved in all four instability mechanisms, the critical Grashof numbers can also be expected to vary with D_1 and D_2 .

Two asymmetric flows that develop for Grashof numbers beyond the critical values are shown in Figs. 4(a) and 4(b), and correspond to $Gr_1 = -3.2$, $Gr_2 = 0$, and $Gr_1 = 0$, $Gr_2 = 18.2$, respectively. The expected distortion of the isoconcentration lines is obvious. The chemical concentration c_2 is shown rather than any of the other variables as species 2 corresponds to the colored oxidized metal ion (M_{ox}) that is observed in experiments.¹²

V. THE SPEED OF THE CONVECTING WAVE

The speeds of the traveling wave solutions are plotted as a function of Grashof numbers in Figs. 5(a) and 5(b). These are ‘‘bifurcation diagrams,’’ in which a measure of the solution, the wave speed, is plotted against a distinguished parameter, the Grashof number. The horizontal lines represent the speed of the nonconvecting wave. These diagrams result from Z_2 -symmetry-breaking bifurcations, and are therefore surprising on two accounts. First, the initial dependence of wave speed on the Grashof number is linear rather than the quadratic behavior that is normally expected near a Z_2 -symmetry-breaking bifurcation point (see, e.g., Golubitsky and Schaeffer¹³). This linear relationship can be explained in terms of the midchannel symmetry.

We parametrize the bifurcating solution branches by an arclength parameter s and seek solution pairs $\mathbf{x}(s)$ and $\lambda(s)$, where $\mathbf{x}(s^0) = \mathbf{x}^0$ and $\lambda(s^0) = \lambda^0$. Differentiating (30) with respect to s ,

$$\frac{\partial \mathbf{f}}{\partial \mathbf{x}} \frac{d\mathbf{x}}{ds} + \frac{\partial \mathbf{f}}{\partial \lambda} \frac{d\lambda}{ds} = \mathbf{f}_{\mathbf{x}} \dot{\mathbf{x}} + \mathbf{f}_{\lambda} \dot{\lambda} = \mathbf{0}. \tag{37}$$

Equation (37) may be satisfied at a simple symmetry-breaking bifurcation point $(\mathbf{x}^0, \lambda^0)$ in one of two ways.

(i) If $\dot{\lambda}(s^0) \neq 0$, then $\dot{\mathbf{x}}(s^0) \in \mathbb{R}_s^N$ and the solution branch lies in \mathbb{R}_s^N .

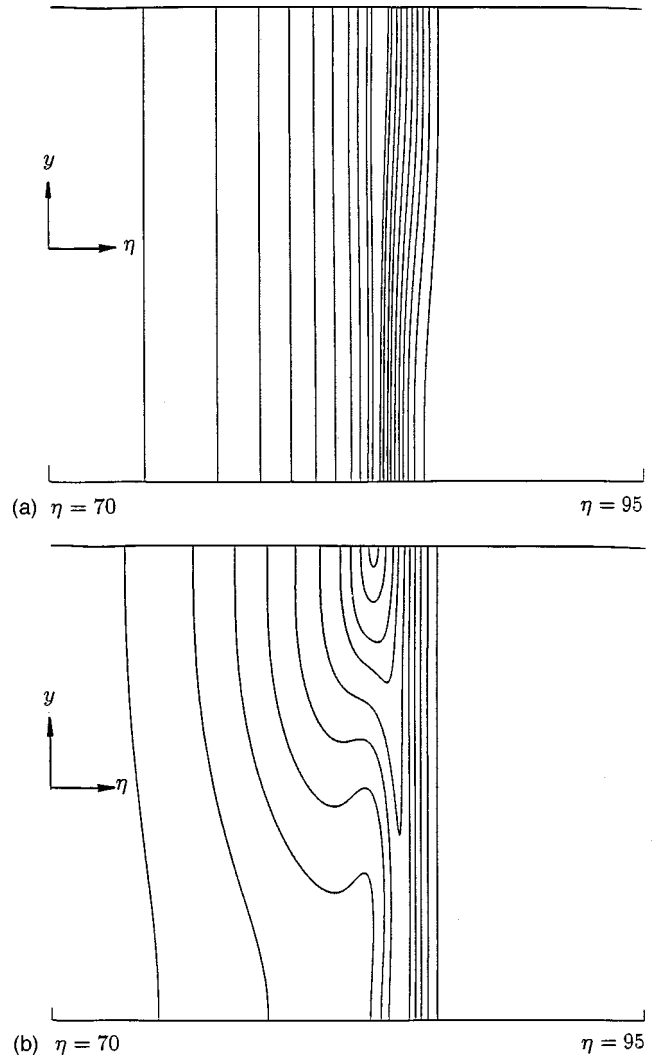


FIG. 4. (a) Isoconcentration lines of c_2 (the scaled M_{ox} concentration) for the convecting solution at $Gr_1 = -3.2$ and $Gr_2 = 0$. Here $\eta \in [70, 95]$, $y \in [-0.5, 0.5]$, and $\epsilon = 0.1$, $D_1 = 1$, $D_2 = 0.6$, $D_\nu = 600$, $f = 3$, $q = 0.0002$, and $\sigma = 2$. Contour values are 0.003, 0.006, 0.009, 0.012, 0.015, 0.018, 0.021, 0.023, 0.025, and 0.026. (b) Isoconcentration lines of c_2 (the scaled M_{ox} concentration) for the convecting solution at $Gr_1 = 0$ and $Gr_2 = 18.2$. Here $\eta \in [70, 95]$, $y \in [-0.5, 0.5]$, and $\epsilon = 0.1$, $D_1 = 1$, $D_2 = 0.6$, $D_\nu = 600$, $f = 3$, $q = 0.0002$, and $\sigma = 2$. Contour values are 0.003, 0.006, 0.009, 0.012, 0.015, 0.018, 0.021, 0.023, 0.025, and 0.026.

(ii) If $\dot{\lambda}(s^0) = 0$, then $\dot{\mathbf{x}}(s^0) = \alpha \phi \in \mathbb{R}_a^N$ and the solution branch cannot lie in the symmetric subspace. We can rescale ϕ so that $\alpha = 1$.

Along the nonsymmetric branches that emerge at a symmetry-breaking bifurcation point, consider $\lambda(x_i)$, where x_i is the i th component of the solution vector \mathbf{x} . By Taylor expansion,

$$\lambda(x_i) = \lambda(x_i^0) + \left. \frac{d\lambda}{dx_i} \right|_{(\mathbf{x}^0, \lambda^0)} (x_i - x_i^0) + \frac{1}{2} \left. \frac{d^2\lambda}{dx_i^2} \right|_{(\mathbf{x}^0, \lambda^0)} (x_i - x_i^0)^2 + \dots$$

Now

$$\frac{d\lambda}{dx_i} = \frac{d\lambda/ds}{dx_i/ds}$$

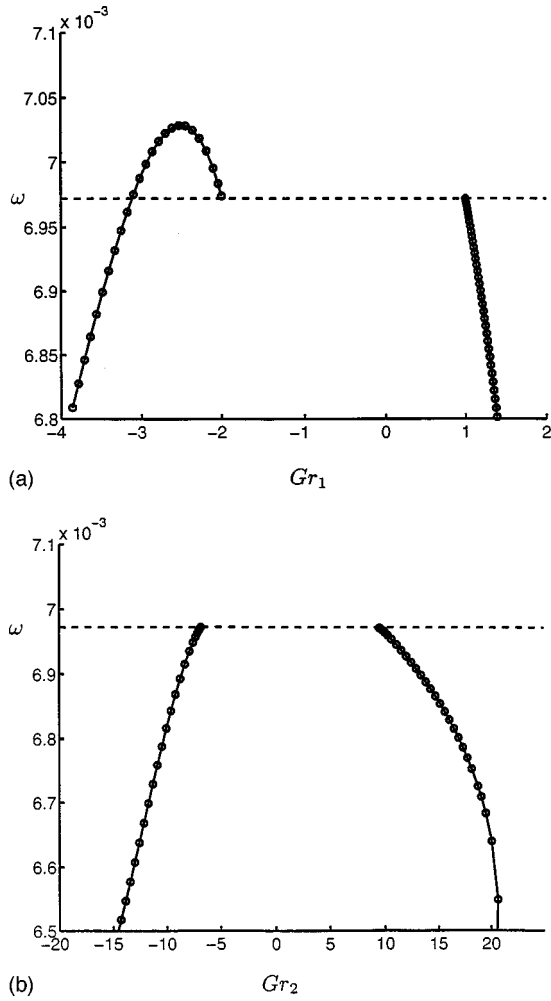


FIG. 5. (a) The speed of the traveling wave solutions as a function of Gr_1 for $Gr_2=0$. The dashed line is the (constant) speed of the nonconvecting solution. The nonconvecting solution is stable for $-1.99 < Gr_1 < 0.998$. Here $\epsilon=0.1$, $D_1=1$, $D_2=0.6$, $D_\nu=600$, $f=3$, $q=0.0002$, and $\sigma=2$. (b) The speed of the traveling wave solutions as a function of Gr_2 for $Gr_1=0$. The dashed line is the (constant) speed of the nonconvecting solution. The nonconvecting solution is stable for $-6.79 < Gr_2 < 9.46$. Here $\epsilon=0.1$, $D_1=1$, $D_2=0.6$, $D_\nu=600$, $f=3$, $q=0.0002$, and $\sigma=2$.

and

$$\left. \frac{d\lambda}{dx_i} \right|_{(x^0, \lambda^0)} = \lim_{s \rightarrow s^0} \frac{d\lambda/ds}{dx_i/ds}.$$

Since $\dot{\lambda}(s^0)=0$, clearly

$$\left. \frac{d\lambda}{dx_i} \right|_{(x^0, \lambda^0)} = 0 \text{ if } \frac{dx_i}{ds}(s^0) = \phi_i \neq 0.$$

Under these circumstances,

$$[\lambda(x_i) - \lambda(x_i^0)] \sim k_1(x_i - x_i^0)^2,$$

which is the expected quadratic dependence at a pitchfork bifurcation point. However, if $(dx_i/ds)(s^0) = \phi_i = 0$, then $d\lambda/dx_i|_{(x^0, \lambda^0)}$ may take some finite nonzero value and

$$[\lambda(x_i) - \lambda(x_i^0)] \sim k_2(x_i - x_i^0).$$

The wave speed components of the solution vector are symmetric about $y=0$ for nonconvecting solutions. The compo-

TABLE II. Linear coefficient α_i and the computed rate of change of wave speed with Grashof number for $D_1=1$, $D_2=0.6$, $D_\nu=600$, $\epsilon=0.1$, $f=3$, $q=0.0002$, and $\sigma=2$.

Gr_1	Gr_2	α_i	Slope
-1.99	0.0	-0.239E-03	-0.234E-03
0.998	0.0	-0.252E-03	-0.866E-03
0.0	-6.79	0.261E-04	0.243E-04
0.0	9.46	-0.109E-04	-0.298E-04

nents of the null eigenvector corresponding to the wave speed must therefore be antisymmetric about $y=0$ at a Z_2 -symmetry-breaking bifurcation point, and necessarily zero along $y=0$. However, because the components of the null eigenvector corresponding to the wave speed must also be constant, they must be zero throughout Ω . The wave speed will therefore vary *linearly* with the bifurcation parameter, be it either the Grashof number Gr_i , $i=1,2$ or the width σ .

In order to calculate $\lim_{s \rightarrow s^0} (dx_i/ds/d\lambda/ds)$ when this form is indeterminate, we must evaluate $\lim_{s \rightarrow s^0} (d^2x_i/ds^2/d^2\lambda/ds^2)$.

We find that

$$\alpha = \lim_{s \rightarrow s^0} \frac{d^2\mathbf{x}/ds^2}{d^2\lambda/ds^2} = \left(\frac{\psi^T \mathbf{f}_{x\lambda}^0 \phi + \psi^T \mathbf{f}_{xx}^0 \mathbf{v}_\lambda \phi}{1/3 \psi^T \mathbf{f}_{xxx}^0 \phi \phi \phi + \psi^T \mathbf{f}_{xx}^0 \mathbf{z} \phi} \right) \mathbf{z} + \mathbf{v}_\lambda,$$

where

$$\mathbf{f}_x^0 \mathbf{v}_\lambda = -\mathbf{f}_\lambda^0, \quad \mathbf{f}_x^0 \mathbf{z} = -\mathbf{f}_{xx}^0 \phi \phi.$$

Let α_i be the i th element of α . Since the wave speed is constant throughout Ω we are free to choose any wave speed component u , say, for which we would need to choose a component that lies on the centerline, at which points the corresponding component of the null eigenvector is necessarily zero.) In Table II, we compare α_i at the four bifurcation points listed in Table I, with the values of the slopes based upon the first point computed along the asymmetric branches.

The second surprising feature of the bifurcation diagrams is that only in one case, that in which the leading edge of the activator wave is unstable, is the wave speed (initially) enhanced by convection. Even this branch has a maximum in the wave speed, and the wave speed of the convecting solution is smaller than the speed of the reaction-diffusion wave for Grashof numbers sufficiently far from the bifurcation point.

An examination of the convecting solutions along the branch for which $Gr_1 < 0$ and $Gr_2 = 0$, shows that the speed of the wave results from a competition between two opposing effects of convection. Convection ahead of the wave enhances diffusion of the activator species into the unreacted medium ahead of the wave, increasing the speed of the wave. Convection, however, also acts to broaden the profiles of both the activator and inhibitor waves, reducing the peak activator concentration. The concentration gradient driving diffusion of the activator species ahead of the wave is thereby reduced, which in turn decreases the speed of the

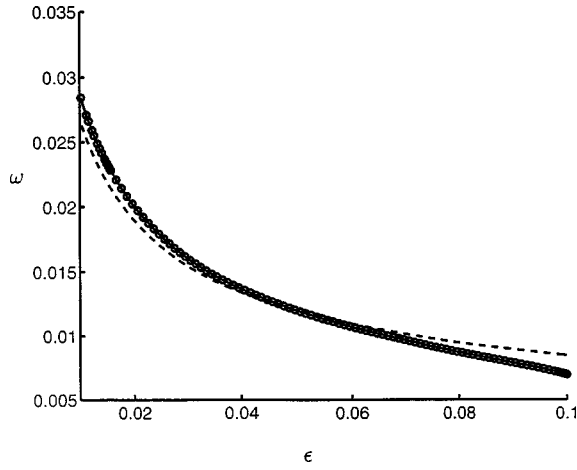


FIG. 6. The speed of the nonconvecting traveling wave solutions as a function of ϵ . The dashed line is $\omega_{rd}(0.05) * \sqrt{0.05/\epsilon}$. Here $D_1=1$, $D_2=0.6$, $D_v=600$, $f=3$, and $q=0.0002$.

wave. The reduction of the rate of diffusion of the activator species ahead of the wave can ultimately outweigh the enhancement due to convective transport.

A maximum wave velocity with Grashof number is not peculiar to the case when $Gr_1 < 0$ and $Gr_2 = 0$. By monitoring the sign of the linear coefficient at the bifurcation point where $Gr_1 = 0$ and $Gr_2 < 0$ as ϵ was varied, we were able to predict the existence of a maximum wave velocity along the bifurcating branch at $\epsilon = 0.095$. This was subsequently verified by direct calculation and the competing effects of convection were evident in the concentration profiles of solutions on either side of the maximum. Similarly, by increasing ϵ to 0.1025, the linear coefficient at the bifurcation point for which $Gr_1 < 0$ and $Gr_2 = 0$ changes sign to become positive, and convection caused by the gravitational instability of the leading edge of the activator wave *always* decreases the speed of the wave.

VI. THE ROLE OF ϵ

In Fig. 6 we show how the speed of the (nonconvecting) reaction-diffusion wave, $\omega_{rd}(\epsilon)$ changes with ϵ . This parameter can, for example, be varied by altering the pH of the reaction mixture. The dashed line is $\omega_{rd}(0.05) * \sqrt{0.05/\epsilon}$, which, following the analysis of Scott,¹² might be expected to approximate this relationship if the wave speed were determined by the autocatalytic step alone. Previous studies have concentrated on values of 0.01 and 0.05 corresponding to the Lo and Hi values of Tyson.¹⁴

The time-dependent equations (1)–(5) were also solved directly using the ENTWIFE package for certain parameter values on a rectangular domain of length L and width 2, with boundary conditions

$$u = v = 0 \text{ on } x = 0 \text{ and } y = \pm 0.5,$$

and

$$\frac{\partial c_i}{\partial n} = 0 \text{ on } x = 0, L \text{ and } y = \pm 0.5.$$

TABLE III. The influence of ϵ on the speed of the nonconvecting reaction-diffusion wave for $D_1=1$, $D_2=0.6$, $D_v=600$, $f=3$, and $q=0.0002$.

ϵ	Wave speed (moving reference frame)	Wave speed (time-dependent calculations)
0.1	2.32 mm/min	2.28 mm/min
0.05	3.99 mm/min	3.73 mm/min
0.01	9.57 mm/min	10.20 mm/min

The initial conditions varied according to the value of ϵ to ensure the system was excitable, and were

$$c_1 = 0.05, \quad 0 \leq x \leq 0.2, \quad \text{for } \epsilon = 0.1,$$

$$c_1 = 0.1, \quad 0 \leq x \leq 0.2, \quad \text{for } \epsilon = 0.05,$$

$$c_1 = 0.8, \quad 0 \leq x \leq 0.2, \quad \text{for } \epsilon = 0.01,$$

with

$$c_1 = 0, \quad 0.2 < x \leq L,$$

and

$$c_2 = \frac{q(f+1)}{(f-1)}, \quad 0 \leq x \leq L.$$

The discretization was performed using quadrilateral elements with quadratic interpolation of the velocity components and continuous linear interpolation of the pressure and species concentrations. A variable step length Gear scheme, with maximum order 5, was used for the time integration.

A comparison of the wave speeds computed at $\epsilon = 0.1$, 0.05, and 0.01 by the two methods appear in Table III, again using $x_0 = 0.018$ cm and $\nu = 0.01$ cm²/s.

The critical Grashof numbers are plotted as a function of ϵ in Figs. 7(a)–7(d). Upon examination of the chemical species profiles of the reaction-diffusion wave, the unexpected maxima and minima in the critical Grashof numbers are seen to correspond (approximately) to minima and maxima in the average concentration gradients at the front and rear of the relevant concentration waves.

There is a complicated relationship between wave speed and ϵ at constant Grashof number, as is evident from Figs. 8(a) and 8(b). In Fig. 8(a), the Grashof numbers are fixed at $Gr_1 = -2$ and $Gr_2 = 0$, so that the front of the activator wave is unstable for all values of ϵ between 0.01 and 0.1. However, the maximum relative increase of the wave speed produced by convection,

$$\Delta \omega^{\text{rel}} = \frac{\omega - \omega_{rd}(\epsilon)}{\omega_{rd}(\epsilon)}$$

[the dashed curve in Figs. 8(a) and 8(b)], does not correspond to the maximum relative distance from the bifurcation point $Gr_1^{\text{crit}}(\epsilon)$,

$$\Delta Gr_1^{\text{rel}} = \frac{Gr_1 - Gr_1^{\text{crit}}(\epsilon)}{Gr_1^{\text{crit}}(\epsilon)}$$

[the dotted curve in Figs. 8(a) and 8(b)]. This suggests a subtle competition between convection's role in transporting

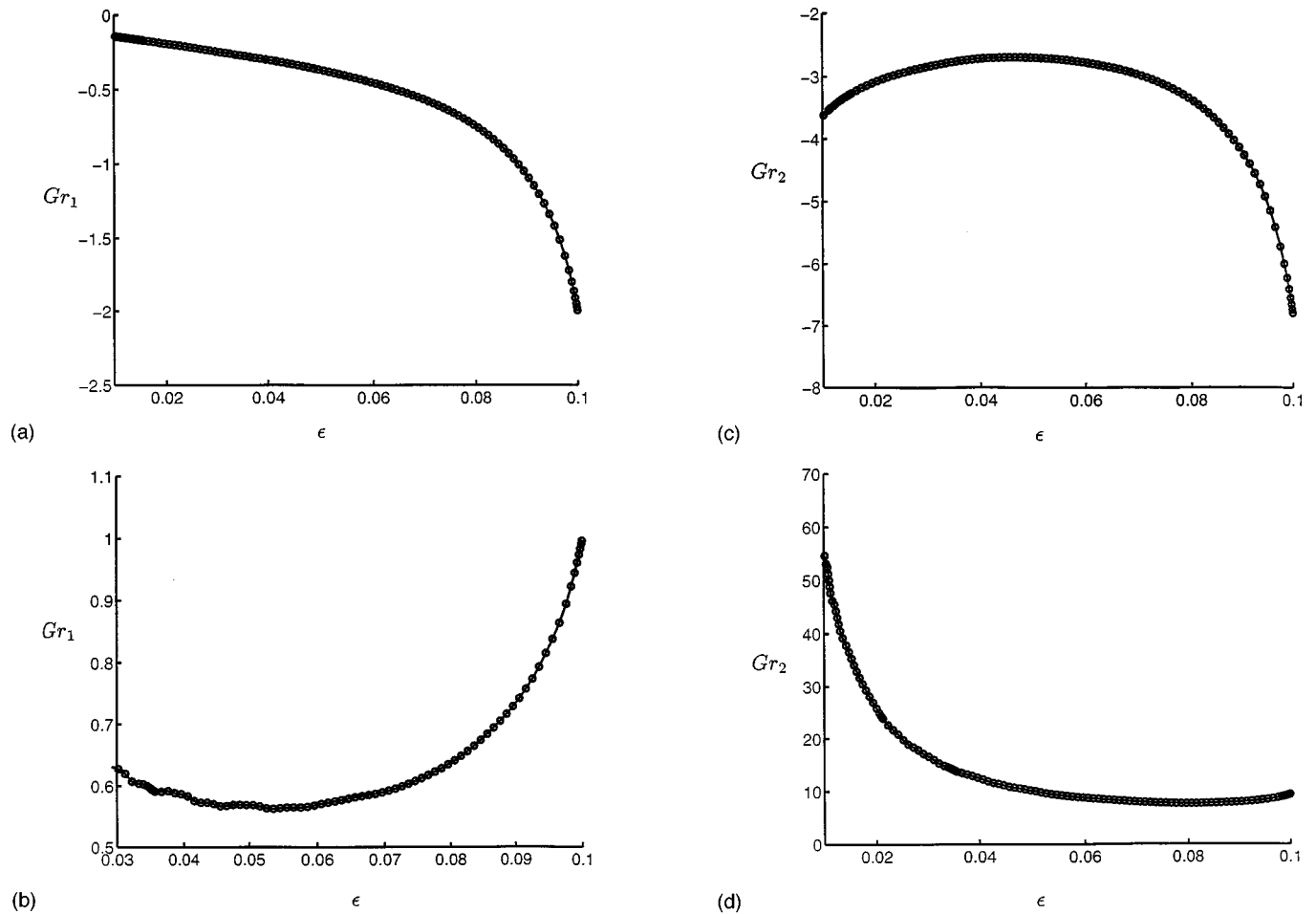


FIG. 7. (a) The critical Grashof number at which the leading edge of the activator wave becomes linearly unstable, as a function of ϵ . Here $Gr_2=0$ and $D_1=1$, $D_2=0.6$, $D_v=600$, $f=3$, $q=0.0002$, and $\sigma=2$. (b) The critical Grashof number at which the trailing edge of the activator wave becomes linearly unstable, as a function of ϵ . Here $Gr_2=0$ and $D_1=1$, $D_2=0.6$, $D_v=600$, $f=3$, $q=0.0002$, and $\sigma=2$. (c) The critical Grashof number at which the leading edge of the inhibitor wave becomes linearly unstable, as a function of ϵ . Here $Gr_1=0$ and $D_1=1$, $D_2=0.6$, $D_v=600$, $f=3$, $q=0.0002$, and $\sigma=2$. (d) The critical Grashof number at which the trailing edge of the inhibitor wave becomes linearly unstable, as a function of ϵ . Here $Gr_1=0$ and $D_1=1$, $D_2=0.6$, $D_v=600$, $f=3$, $q=0.0002$, and $\sigma=2$.

the activator species ahead of the wave and reducing the diffusion ahead of the wave by spreading the wave and reducing the concentration gradients.

In Fig. 8(b), the Grashof numbers are fixed at $Gr_1=1.5$ and $Gr_2=0$, so that the tail of the activator wave is unstable for all values of ϵ between 0.03 and 0.1. For $0.06 < \epsilon < 0.1$ convection slows the wave, but for $\epsilon < 0.06$ the wave speed is marginally enhanced. As ϵ decreases toward 0.03 and the activator wave steepens, diffusion of the activator species ahead of the wave dominates the wave speed since the convection behind the wave has very little influence on the speed of the wave. The curves of the wave speeds for the convecting and nonconvecting solutions are virtually coincident. We suspect that such subtle differences in velocity would be very difficult to detect via time-dependent computations or to observe experimentally.

Time-dependent computations were performed for $\epsilon=0.01$, $f=3$, $q=0.0002$, $D_1=1.0$, $D_2=0.6$, $D_v=600$, $\sigma=2$, and $L=40$, in order to demonstrate the changes in wave speed produced in the four different instability scenarios.

For this value of ϵ , convection in front of the wave initiated by the activator ($Gr_1 < 0$) or inhibitor ($Gr_2 < 0$) steepens the leading edge of the activator pulse without decreasing its magnitude and therefore increases the wave speed. Wilke⁸ reports the same behavior for chemical waves traveling in horizontal domains. On the other hand, convection behind the wave lowers the peak concentrations, decreasing the total diffusion of the activator species ahead of the wave and slows the wave. A selection of wave speeds are presented in Table IV. The wave speeds were of course determined only once the initial transience had decayed and the waves had attained their final shape.

The streamlines and isoconcentration contours depend upon the nature of the instability. Figures 9(a) and 9(b) illustrate streamlines and isoconcentration lines for two of the cases given in Table IV. Because of the long tail of the inhibitor wave, flow is generated far behind the leading edges of the waves.

In Fig. 9(a), for which $Gr_1 = -0.5$ and $Gr_2 = 0$, the convective roll initiated by the concentration gradient in the front of the activator wave initiates a secondary vortex be-

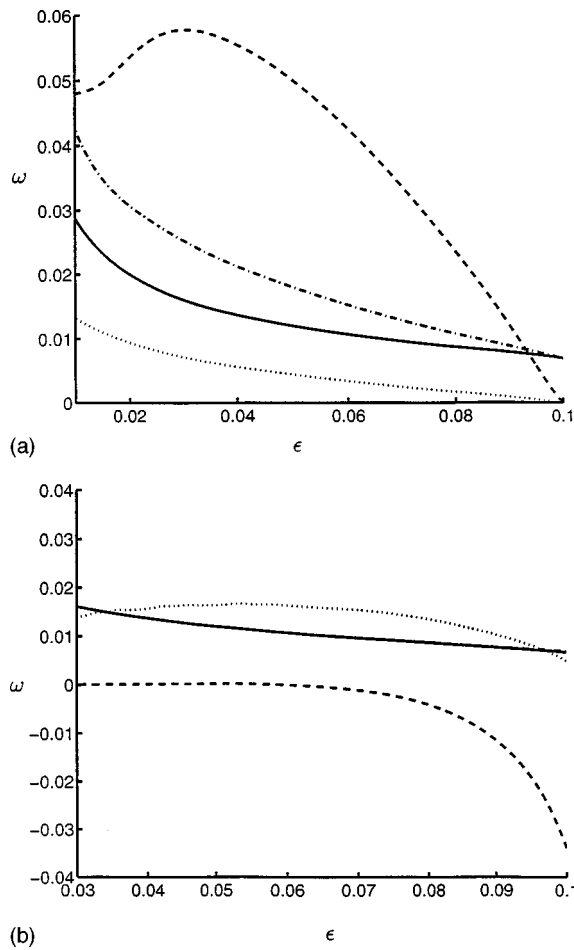


FIG. 8. (a) Wave speed versus ϵ for $Gr_1 = -2.0$, $Gr_2 = 0$. (—), nonconvecting solution; (---), convecting solution; (---), 0.1* relative increase in wave speed; (···), 0.001* relative distance of Gr_1 from critical. (b) Wave speed versus ϵ for $Gr_1 = -1.5$, $Gr_2 = 0$. (—), nonconvecting solution; (---), convecting solution; (---), relative increase in wave speed; (···), 0.01* relative distance of Gr_1 from critical.

hind the two concentration waves. This is expected from the null eigenvector shown in Fig. 2(a). The solution at $Gr_1 = 0$ and $Gr_2 = 80$, shown in Fig. 9(b), has a single vortex behind the two waves. This is again predicted by the null eigenvector shown in Fig. 2(d).

TABLE IV. Some wave speeds of convecting solutions for $D_1 = 1$, $D_2 = 0.6$, $D_v = 600$, $\epsilon = 0.01$, $f = 3$, $q = 0.0002$, and $\sigma = 2$.

Gr_1	Gr_2	Wave speed (mm/min)
0.0	0.0	10.2
-0.5	0.0	11.5
-2.0	0.0	13.3
+2.0	0.0	8.3
0.0	-30.0	12.3
0.0	-40.0	17.4
0.0	+80.0	7.8
0.0	+200.0	6.5

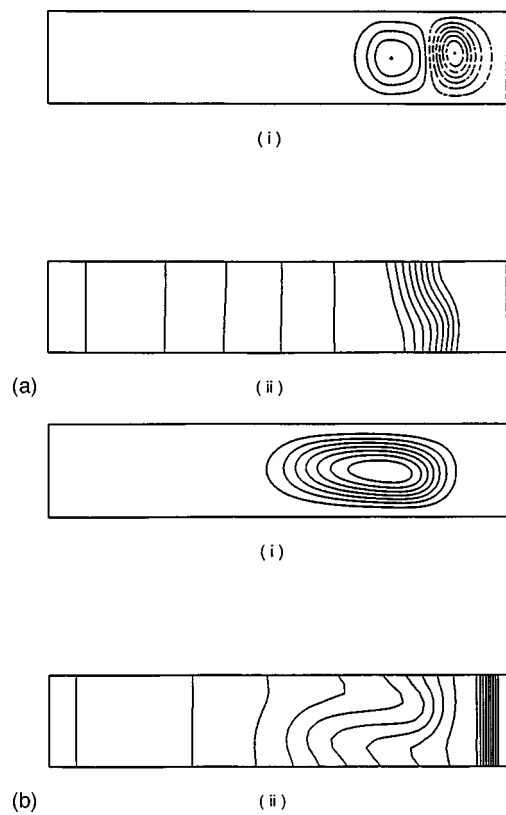


FIG. 9. (a) The traveling wave solution for $Gr_1 = -0.5$, $Gr_2 = 0$. Here $D_1 = 1$, $D_2 = 0.6$, $D_v = 600$, $\epsilon = 0.01$, $f = 3$, $q = 0.0002$, $\sigma = 2$, and $L = 40$. (i) streamlines; (ii) isoconcentration lines of c_2 . (b) The traveling wave solution for $Gr_1 = 0$, $Gr_2 = 80$. Here $D_1 = 1$, $D_2 = 0.6$, $D_v = 600$, $\epsilon = 0.01$, $f = 3$, $q = 0.0002$, $\sigma = 2$, and $L = 40$. (i) streamlines; (ii) isoconcentration lines of c_2 .

VII. SUMMARY

A commonly used excitable BZ reaction system was investigated numerically. The interaction between the chemical kinetics and diffusion produces a reaction front, also called a chemical wave or pulse, which propagates into the unreacted medium. The BZ reaction kinetics were approximated using the two-component Oregonator model. This model was coupled with the equations of motion of a Newtonian fluid and investigated in a vertical two-dimensional channel using the finite-element method. In sufficiently narrow channels, the onset of convection was shown to occur as a symmetry-breaking bifurcation from the nonconvecting solution.

Depending upon the channel orientation and the chemical species present, four distinct instability mechanisms can occur. The linear dependence of wave speed on channel width that has been observed in experiments, has been shown to be a consequence of the Z_2 symmetry breaking that is associated with the onset of convection in sufficiently narrow channels. Unlike the behavior of horizontally traveling chemical waves, convection does not necessarily increase the speed of the wave. Steady, as well as time-dependent calculations have shown that for particular reaction mixtures, convection increases the speed of ascending waves but decreases the speed of descending waves. The latter is an interesting new feature and arises because convection behind the pulse lowers the peak concentrations and therefore decreases dif-

fusion ahead of the wave. The reaction time scale ϵ was varied in the range 0.01–0.1 in order to investigate the influence of pulse shape on the critical conditions for convection and on the convecting and nonconvecting wave speeds.

By recasting the equations of motion in a moving reference frame and using an extended system technique to locate symmetry-breaking bifurcation points, we have developed an efficient technique for locating the critical conditions at which convection arises. Our approach makes an exploration of the multidimensional parameter space feasible. Just as the location of the bifurcation points for a range of values of ϵ was computed, so continuation with respect to the diffusion parameters or any of the coefficients in the Oregonator model can be performed. An extensive study has not yet been attempted as, given the large number of independent parameters, such a study is best performed in conjunction with laboratory experiments, and is currently being planned. Invoking results from singularity theory, we expect the qualitative nature of the bifurcation diagrams to remain unchanged for “small” changes of the parameters, since their qualitative nature can only change at higher codimension singularities. Unfortunately the location of such high-order singular behavior must be determined by computation. Quantitative information, such as the effect of ϵ on the critical Grashof numbers and on the wave speed as presented in Figs. 7 and 8, can only be obtained numerically. Symmetry arguments alone were used to explain the initial linear dependence of wave speed on the bifurcation parameter, so this behavior should be observed for all convecting flows arising at *symmetry-breaking* bifurcation points.

ACKNOWLEDGMENTS

K. A. Cliffe and S. J. Tavener would like to thank the British Council for supporting this work under the British–German academic research collaboration (ARC) programme, Project No. 468, and gratefully acknowledge the continuing

support of AEA Technology. H. Wilke would like to acknowledge the support of the Deutsche Forschungsgemeinschaft (DFG) and the Deutscher Akademischer Austauschdienst (DAAD). S. J. Tavener would also like to acknowledge the support of the Oxford University Computing Laboratory and to thank Professor S. K. Scott of the University of Leeds for useful discussions.

- ¹G. Bazsa and I. R. Epstein, “Traveling waves in the Nitric-Iron(II) reaction,” *J. Phys. Chem.* **89**, 3050 (1985).
- ²J. A. Pojman and I. R. Epstein, “Convective effects on chemical waves. I. Mechanisms and stability criteria,” *J. Phys. Chem.* **94**, 4966 (1990).
- ³J. Masere, D. A. Vasquez, B. F. Edwards, J. W. Wilder, and K. Showalter, “Nonaxisymmetric and axisymmetric convection in propagating reaction-diffusion fronts,” *J. Phys. Chem.* **98**, 6505 (1994).
- ⁴Y. Wu, D. A. Vasquez, B. F. Edwards, and J. W. Wilder, “Convective chemical-wave propagation in the Belousov–Zhabotinsky reaction,” *Phys. Rev. E* **51**, 1119 (1995).
- ⁵D. M. Zhang, W. R. Peltier, and R. L. Armstrong, “Buoyant convection in the Belousov–Zhabotinsky reaction. II. Chemically driven convection and instability of the wave structure,” *J. Chem. Phys.* **103**, 4078 (1995).
- ⁶W. Janke, W. E. Skaggs, and A. T. Winfree, “Chemical vortex dynamics in the Belousov–Zhabotinsky reaction and in the two-variable Oregonator model,” *J. Phys. Chem.* **93**, 740 (1989).
- ⁷M. Böckmann, B. Hess, and S. C. Müller, “Temperature gradients traveling with chemical waves,” *Phys. Rev. E* **53**, 5498 (1995).
- ⁸H. Wilke, “Interaction of traveling chemical waves with density driven hydrodynamic flows,” *Physica D* **86**, 508 (1995).
- ⁹K. A. Cliffe, “ENTWIFE (Release 6.3) Reference Manual: ENTWIFE, INITIAL DATA and SOLVER DATA Commands,” AEAT-0823, 1996.
- ¹⁰B. Werner and A. Spence, “The computation of symmetry-breaking bifurcation points,” *SIAM (Soc. Ind. Appl. Math.) J. Numer. Anal.* **21**, 388 (1984).
- ¹¹A. C. Hearn, “REDUCE users manual,” Rand Publication CP78, 1987.
- ¹²S. K. Scott, “Oscillations, waves and chaos in chemical systems,” *Oxford Chemistry Primers* (Oxford University Press, Oxford, 1994).
- ¹³M. Golubitsky and D. G. Schaeffer, *Singularities and Groups in Bifurcation Theory* (Springer-Verlag, New York, 1984), Vol. 1.
- ¹⁴J. J. Tyson, “A quantitative account of oscillations, bistability, and traveling waves in the Belousov–Zhabotinsky reaction,” in *Oscillations and Traveling Waves in Chemical Systems*, edited by R. J. Field and M. Burger (Wiley, New York, 1985).